ISSN 0036-0295, Russian Metallurgy (Metally), Vol. 2021, No. 8, pp. 1029–1035. © Pleiades Publishing, Ltd., 2021.
Russian Text © The Author(s), 2021, published in Rasplavy, 2021, No. 3, pp. 303–314.

# Electrochemical Synthesis of Titanium Oxide Nanopowders in a Molten Mixture of Alkali Chlorides and Nitrates

**L. A. Elshina[a], *, A. G. Kvashnichev[a], and D. V. Pelegov[b]**

[a] *Institute of High-Temperature Electrochemistry, Ural Branch, Russian Academy of Sciences, Yekaterinburg, Russia*
[b] *Ural Federal University named after the First President of Russia B.N. Yeltsin, Yekaterinburg, 620002 Russia*
**e-mail: yolshina@ihte.uran.ru*

Received January 12, 2021; revised January 29, 2021; accepted February 1, 2021

**Abstract**—Titanium oxide nanoparticles are synthesized in a molten mixture of alkali chlorides and nitrates. X-ray diffraction analysis, Raman spectroscopy, and scanning electron microscopy are used to identify the oxide powders. Titanium oxides of various modifications and compositions are synthesized by anodic polarization of high-purity titanium in a molten eutectic mixture of cesium and sodium chlorides containing 5 wt % sodium nitrate. Polarization is carried out under galvanostatic conditions at a current density of 3.5 mA/cm$^2$ and a temperature of 540–700°C in an argon atmosphere. The phase composition of the oxidation products depends on the synthesis temperature. The particle size is controlled by varying the density and temperature. X-ray diffraction analysis and Raman spectroscopy show that the sample synthesized at a temperature of 540°C is single-phase and consists of $Cs_{1.36}Ti_{6.64}O_{16}$. The samples synthesized at temperatures of 600 and 650°C form the $TiO_2$ phase in mixed anatase and rutile modifications. The sample synthesized at a temperature of 700°C consists of $TiO_2$ titanium dioxide (rutile and brookite modification) and $NaTi_8O_{13}$. According to scanning electron microscopy, the particle size decreases when the synthesis temperature increases. The sample synthesized at a temperature of 540°C and annealed at a temperature of 200°C contains a mixture of the nano- and microparticles of cesium trititanate (over 50 nm). The titanium dioxide particle size is 20 nm in the sample synthesized at a temperature of 600°C and is 10–20 nm in the samples synthesized at temperatures of 650 and 700°C.

**Keywords:** nanocrystalline titanium oxide, molten salts, anodic polarization, titanium

**DOI:** 10.1134/S0036029521080061

## INTRODUCTION

Titanium dioxide is currently used as a pigment in the paint and varnish industry (white titanium), in the manufacture of paper, synthetic fibers, plastics, rubber products, ceramic dielectrics, heat-resistant and optical glass (including fiber optics), as a component of electrode coating for electric welding and casting mold coatings. However, researchers pay close attention to the photocatalytic properties of titanium dioxide, in particular, to its possible application to solar cells [1–3]. The photocatalytic properties are known to be most pronounced when titanium dioxide is in the form of nanocrystalline particles [4]. Therefore, the influence of the technique of producing titanium dioxide nanoparticles on the catalytic properties has been studied extensively. The use of titanium dioxide nanopowders makes the cost of 1 kWh five times lower as compared to analogs based on silicon semiconductor materials. In addition, titanium nanodioxide is used in the space industry and for the production of special synthetic materials for UV protection, self-cleaning glasses [5–7], wastewater photocatalysts [8, 9], electrochromic displays, and hydrogen extraction during water splitting [10–12].

The main methods of producing titanium nanoxide are the traditional sol-gel [13–15], hydrothermal, and solvothermal syntheses [16–18]. X-ray amorphous or crystalline $TiO_2$ in the form of rutile, anatase, or their mixture is synthesized depending on the processing conditions.

Molten salt synthesis (MSS) is a simple technique to synthesize simple and complex oxides of the desired composition. Molten salts, such as alkali metal chlorides, nitrates, and sulfates, are often used as reaction media or solvents for chemical reactions, since the diffusion rates of the components in molten salts are much higher than in the solid state. Consequently, the annealing temperature should not affect the MSS significantly.

Many metal oxides can be deposited from molten salts [19–21]. Several factors make molten salts an attractive medium for oxide synthesis. They include other ways to form oxides of the desired morphology that cannot or are too difficult to obtain by the above-mentioned techniques, a wider range of oxidation

temperatures, and a greater variety of possible chemical reactions. In addition, the reactions when metals interact with molten salts are usually much faster than they are in solids. The lower melting temperatures of molten nitrates as compared to those of other ionic melts and their thermal instability make them unsuitable for the growth of perfect crystals. However, powders with a highly developed surface were synthesized in these media ($ZrO_2$, $Al_2O_3$, PbO, $TiO_2$) [22–26].

The synthesis of titanium dioxide nanopowders, which can be carried out by titanium oxidation in chloride–nitrate melts under different conditions, is now of great practical importance [27]. The corrosion-electrochemical behavior of titanium in molten chloride–nitrate electrolyte was studied in [28].

Earlier, we showed that loose defective titanium oxide films of nonstoichiometric composition with low oxygen content (52 at % titanium, 48 at % oxygen) formed on the titanium surface under both no-current and anodic polarization conditions in the CsCl–NaCl melt containing sodium nitrate up to ~5 wt %. Significant amounts of titanium oxide (more than 0.5 g per 50 g melt during a single experiment) formed in form of both nano- and micrograined powders in the volume of the salt electrolyte. The powders formed during no-current titanium oxidation were characterized by different particle sizes, from 1 nm (about 2%) to 2–3 μm.

Monodisperse oxide powders are known to be of particular value for practical applications. This synthesis needs oxidation in the anodic polarization mode. Anodic polarization curves of titanium in a CsCl–NaCl melt containing from 1 to 10 wt % sodium nitrate were recorded at 540–700°C to select the current density at which monodisperse powders form. The anodic current density at which titanium oxide nanopowders formed is 3.5 mA $cm^{-2}$.

Analysis of the literature data suggests that the electrochemical synthesis of titanium oxide in molten salts can solve the problem of controlling the particle size and the morphology of the resultant nanooxide.

This work aims to study the morphology and phase composition of titanium dioxide and titanium-based complex oxide nanopowders formed by controlled electrochemical synthesis in a molten eutectic mixture of cesium and sodium chlorides containing 5 wt % sodium nitrate over a wide temperature range in an argon atmosphere.

## EXPERIMENTAL

$TiO_2$ samples were synthesized by the anodic polarization of high-purity titanium in a molten eutectic mixture of cesium and sodium chlorides, containing 5 wt % sodium nitrate. The polarization was carried out in an Autolab 302N potentiostat/galvanostat under galvanostatic conditions at a current density of 3.5 mA/$cm^2$ in the temperature range 540–700°C and an argon atmosphere. The powder synthesized at 540°C was subjected to additional annealing at 200°C for 2 h.

Titanium anodes were placed in the melt only after reaching the desired temperature to prevent the formation of coarse titanium oxide crystals during the no-current period of the experiment.

The synthesis time was chosen experimentally according to the type of galvanostatic curve. The potential fluctuations were small on the galvanostatic curve due to the formation of titanium oxide nanopowders on the titanium surface. The synthesis was stopped after a sudden potential jump was observed on the curve.

The salt fusion cake after the experiment was cooled to room temperature, milled, and dissolved in distilled water.

The finely dispersed precipitate was filtered or centrifuged, washed in distilled water many times, and dried either in the air or in an oven at 200°C.

X-ray diffraction (XRD) analysis, Raman spectroscopy, and electron microscopy were used to investigate the powders. XRD analysis was performed using a Bruker D8 Discover diffractometer in the range $5° \le 2\theta \le 80°$. Phase analysis was conducted with the PDF-2 ICDD (2010) database. Raman spectroscopy was carried out on an Integra Spectra spectroscope in the Raman frequency range from 100 to 1000 $cm^{-1}$. Electron microscopy images of the synthesized powders were taken with a Carl Zeiss Workstation AURIGA GrossBeam electron microscope (Germany).

## RESULTS AND DISCUSSION

Figure 1 shows the typical polarization curves recorded for titanium anodes in the CsCl–NaCl–5% $NaNO_3$ melt at temperatures of 600 and 650°C.

The anodic polarization curves taken under galvanostatic conditions were used to determine the synthesis time. At the beginning of polarization, there is a potential shift toward negative values due to the formation of titanium dioxide powders, which are poorly bonded to the metal base. The serrated curve corresponds to the formation of poorly bonded titanium oxide and its spalling into the molten salt. The sharp potential jump in the positive direction indicates the formation of a protective oxide layer on the titanium surface and, consequently, the end of synthesis. As the synthesis temperature increased, the time decreased from 5 h at 540°C to 1.5 h at 700°C.

The potentials of the titanium anode during polarization shift to positive values when the synthesis temperature increases, which can indicate a change in the phase composition of the synthesis product.

Electron microscopy images of the nanopowders synthesized by anodic polarization of titanium in nitrate chloride melt are shown in Fig. 2.

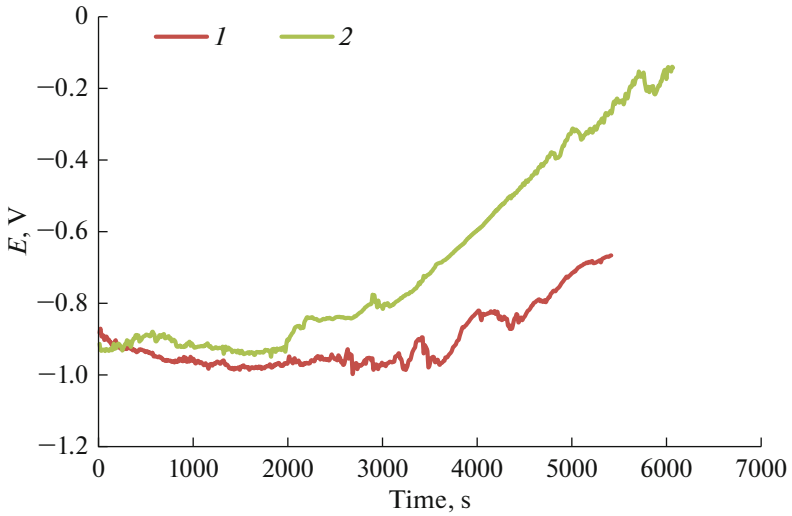


**Fig. 1.** Polarization curves of the samples synthesized at temperatures of (*1*) 600 and (*2*) 650°C in the CsCl–NaCl–5 % $NaNO_3$ melt.

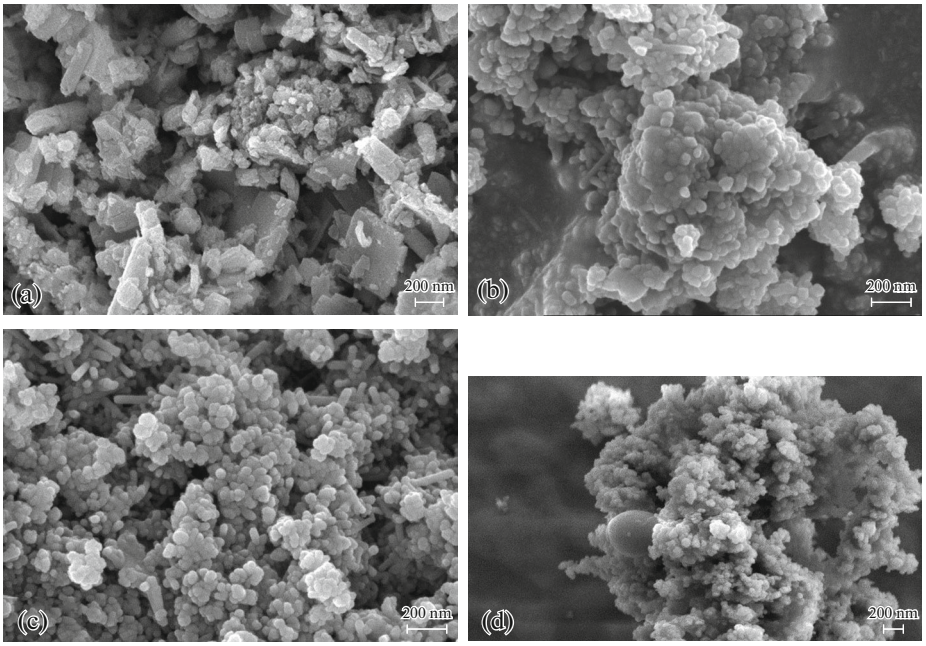


**Fig. 2.** SEM images of the powders synthesized at (a) 540, (b) 600, (c) 650, and (d) 700°C in the CsCl–NaCl–5 % $NaNO_3$ melt.

One can see that the powder synthesized at 540°C is a mixture of nano- (up to 50 nm) and microparticles (Fig. 2). Their sizes can be explained by particle agglomeration during annealing carried out to remove water from the powder. The particle size in the powders prepared at 600 and 650°C is close to 20 nm. This size is much smaller than that in the previous samples, because those powders were not annealed. A temperature increase to 650°C resulted in the formation of nanotubes in the powder. Titanium oxide nanopowders produced at 700°C were dissolved in distilled water to produce stable suspensions of nanopowders. We failed to deposit them at 6000 rpm in a high-speed centrifuge for 6 h. The upper part of the solutions with the nanopowder, which was retained as an opalescent solution for several months, was poured off. The lower part was pipetted into Petri dishes and left there to dry. The largest titanium dioxide particles formed in this experiment, up to 10 nm in size, can be seen in the electron microscopy images. All particles look like crystallites with clear angles. Therefore, we can conclude that an increase in the synthesis temperature causes a significant decrease in the oxide powder particle size.

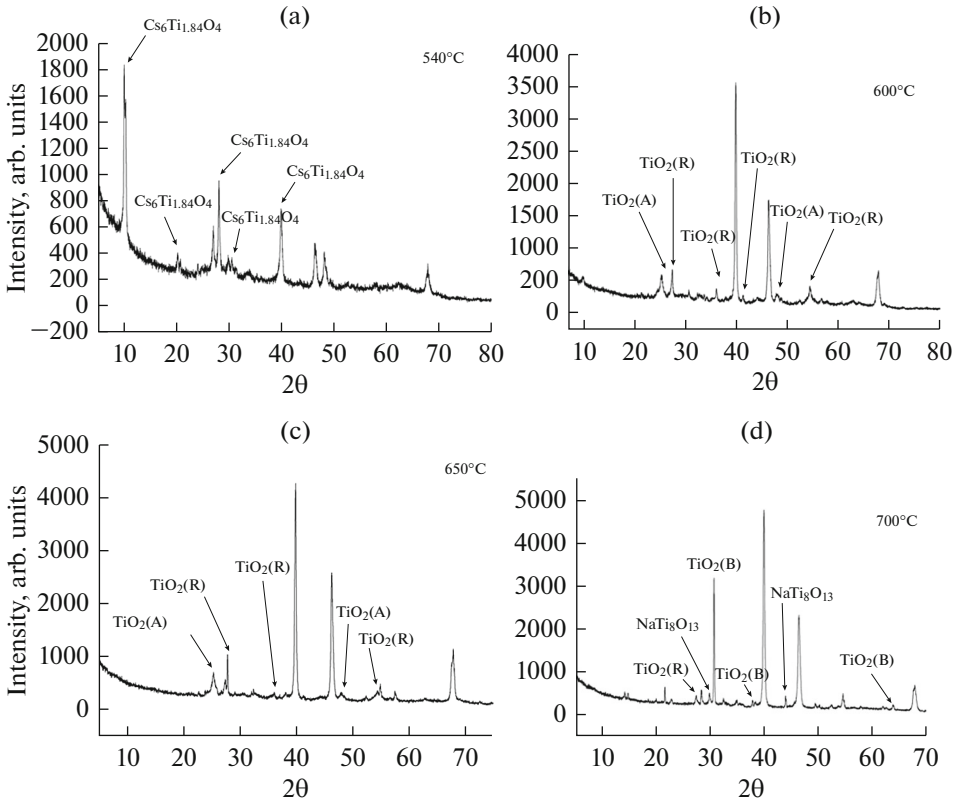


**Fig. 3.** XRD patterns of the samples synthesized at (a) 540, (b) 600, (c) 650, and (d) 700°C in the CsCl–NaCl–5 % $NaNO_3$ melt. The unmarked peaks belong to the substrate.

The oxide phase was identified by XRD analysis. All the peaks in the XRD patterns presented in Fig. 3 are well pronounced and have no broadening, which can be attributed to a high degree of crystallinity in the titanium oxide nanopowders formed during synthesis.

The powder synthesized at 540°C and annealed at 200°C is cesium trititanate with characteristic peaks at $2\theta = 20.8°$, 27.9°, 31.7°, and 40° (Fig. 3a). We could not find references to synthesis of this compound in the literature and assume that it is isostructural with sodium trititanate, which is a very promising material for chemical current sources.

The powder electrochemically synthesized at 600°C consists of the $TiO_2$ phase with the prevailing rutile modification (lines at $2\theta = 27.45°$, 37.9°, 41.2°, 54.34°) and an admixture of minor anatase peaks at $2\theta = 25.23°$ and 47.57° (Fig. 3b).

The XRD pattern of the sample synthesized at 650°C exhibits high peak intensities at $2\theta = 27.45°$, 37.9°, and 54.34° and, consequently, an increase in the amount of the rutile phase; anatase modification is also present at $2\theta = 25.23°$ and 47.57° but in a smaller amount.

The oxide powder synthesized at 700°C is multiphase. The predominant phase with very high intensities at $2\theta = 30.814°$, 37.819°, and 63.629° in an XRD pattern is the brookite. There is no anatase at all, and the impurity phases are rutile with a peak at $2\theta = 27.390°$ and $NaTi_8O_{13}$ with characteristic peaks at $2\theta = 29.760°$ and 43.929°. The $NaTi_8O_{13}$ phase, which is a sodium titanate with a mixed valence of titanium $Ti^{3+}/Ti^{4+}$, was synthesized by Akimoto in 1991 for the first time [29]. The main phase in the powder is titanium dioxide in the brookite modification.

Therefore, we can conclude that an increase in the electrochemical synthesis temperature from 540 to 700°C changes not only the particle size and morphology of the oxide nanopowder, but also its phase composition.

In addition, the oxide powders were identified by Raman spectroscopy (Figs. 5, 6).

The Raman spectrum of the powder synthesized at 540°C exhibits peaks at Raman bands of 272, 444, and 697 $cm^{-1}$, which are similar to those of sodium trititanate available in the literature. Raman spectroscopy of the sample prepared at 600°C shows characteristic peaks of the $TiO_2$ anatase modification at Raman bands of 147, 398, 515, and 640 $cm^{-1}$. The domination of anatase is known to indicate a small particle size due to the higher stability of titanium nanooxide in the anatase modification as compared to rutile.

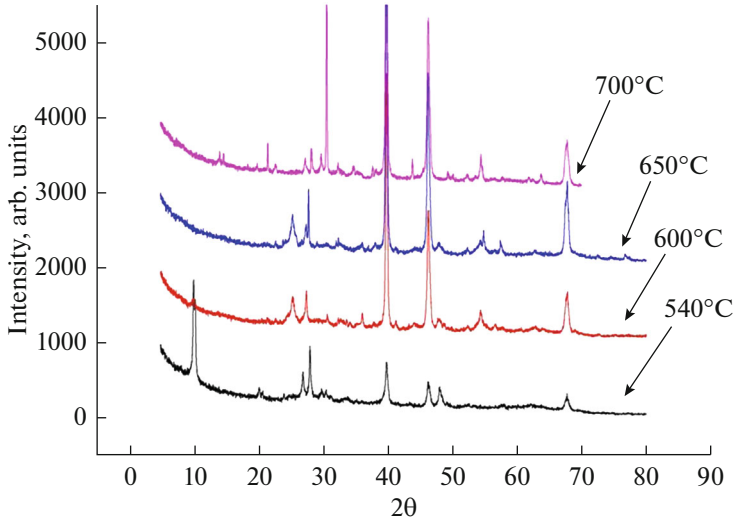


**Fig. 4.** Comparative XRD patterns of the titanium oxide samples synthesized at different temperatures.

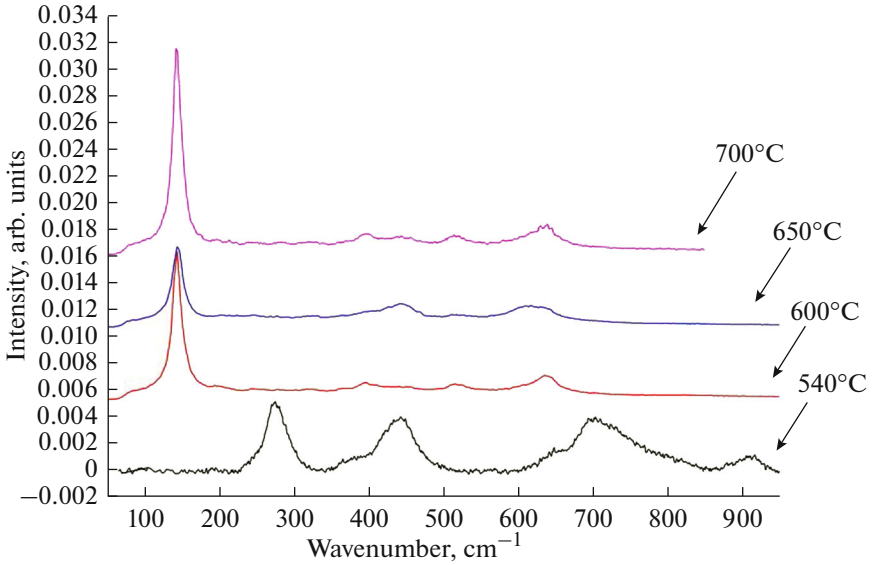


**Fig. 5.** Raman spectra of the powders synthesized at 540, 600, 650, 700°C in the CsCl–NaCl–5% $NaNO_3$ melt.

Raman spectroscopy of the nanopowder sample synthesized at 650°C shows two $TiO_2$ modifications, namely, anatase and rutile. The rutile fraction is minimal and its characteristic peak is at 448 cm$^{-1}$.

The main peaks of anatase are in the same Raman bands as those of the sample prepared at 600°C.

Raman spectra of the sample prepared at 700°C were recorded at different points, since XRD analysis showed a multiphase structure of the sample. Figure 6 depicts the spectrum of single-phase $TiO_2$ with the rutile modification. The combination bands are at 144, 448, and 612 cm$^{-1}$. Figure 5 displays peaks of all three main modifications, namely, rutile, anatase, and brookite. The combination bands of rutile are located similar to those of the sample synthesized at 600°C. Anatase was detected at 620 cm$^{-1}$. Brookite exhibits a relatively complex vibration spectrum with the main bands at 398, 440, and 512 cm$^{-1}$.

Additional annealing of titanium oxide nanopowders results in the agglomeration of particles and, consequently, an increase in their size.

Synthesis of metal oxide nanopowders, including titanium oxide, using anodic polarization of metals in a molten nitrate chloride electrolyte should be referred to dispersion techniques (“top-down”), which are used rather rare in chemistry: anodic activation causes metal ionization, and a formed $M^{n+}$ ion reacts rapidly with oxygen-containing ions in the liquid salt phase.

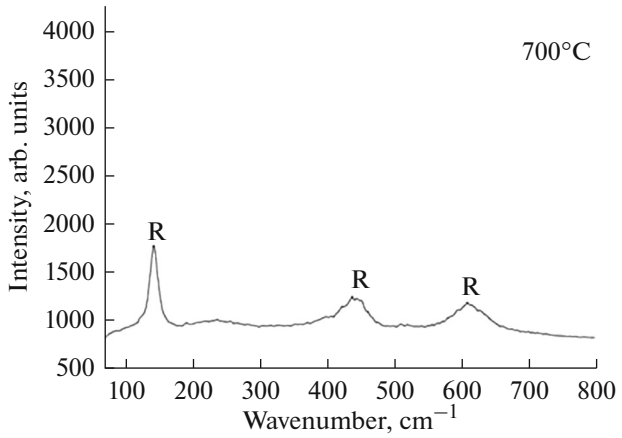


**Fig. 6.** Raman spectrum of single-phase $TiO_2$ with the rutile modification.

The concentration of metal ions in the melt can be controlled by changing the current density. The concentration of metal ions, along with the concentration of oxygen-containing ions, is responsible for the rate of new phase formation. This allows us to control the rate of the chemical reaction, the nucleation process, and, consequently, the particle size of the resultant powders. The synthesis temperature controls the phase composition of the products of titanium oxidation in the chloride–nitrate melt. An increase in the synthesis temperature also reduces the particle size in the nanopowders.

Titanium dioxide in the rutile modification synthesized by the electrochemical technique in molten salts at 600°C was subsequently used to synthesize Al–$Al_2O_3$ nanocomposites [30].

## CONCLUSIONS

The anodic polarization of titanium at temperatures of 540–700°C in the galvanostatic mode in the molten eutectic mixture of cesium and sodium chlorides (5 wt %) synthesizes titanium oxide nanopowders in the salt electrolyte volume and a dense protective titanium oxide layer on the surface of a titanium anode. The formation of the layer stops nanopowder synthesis in the electrolyte volume.

The synthesis temperature is shown to affect the phase composition of the titanium oxide nanopowders. The nanopowder synthesized at 540°C consists of a single phase, $Cs_{1.36}Ti_{6.64}O_{16}$, and the nanooxides synthesized at 600 and 650°C form the $TiO_2$ phase in mixed modifications (anatase, rutile).

The sample synthesized at a temperature of 700°C consists of $TiO_2$ titanium dioxide (rutile and brookite modification) and $NaTi_8O_{13}$ impurity sodium titanium oxide. All the formed nanopowders are highly crystalline.

The morphology of the nanopowder can be successfully controlled by changing the current density and the temperature; in particular, the crystal size decreases from 50 to 20 nm when the temperature increases from 540 to 700°C.

## REFERENCES

1. C. Ma, L. Wang, Z. Guo, Y. Lv, W. Chen, H. Ming, P. Ma, and J. Wang, Colloids Surf. A **538**, 94–99 (2018). https://doi.org/10.1016/j.colsurfa.2017.10.089
2. X. Liu, C. Zhang, S. Liu, and Y. Xiong, Optik (Stuttg) **160**, 277–282 (2018). https://doi.org/10.1016/j.ijleo.2018.02.008
3. S. V. Umale, S. N. Tambat, V. Sudhakar, S. M. Sontakke, K. Krishnamoorthy, Adv. Powder Technol. **28**, 2859–2864 (2017). https://doi.org/10.1016/j.apt.2017.08.012
4. P. Ilaiyaraja, T. Kumar Das, P.S.V. Mocherla, and C. Sudakar, Sol. Energy Mater. Sol. Cells. **169**, 86–97 (2017). https://doi.org/10.1016/j.solmat.2017.05.001
5. D. Adak, S. Ghosh, P. Chakrabarty, A. Mondal, H. Saha, R. Mukherjee, and R. Bhattacharyya, Sol. Energy. **155**, 410–418 (2017). https://doi.org/10.1016/j.solener.2017.06.014
6. R. J. Isaifan, A. Samara, W. Suwaileh, D. Johnson, W. Yiming, A. A. Abdallah, and B. Aïssa, Sci. Rep. **7**, 9466 (2017). https://doi.org/10.1038/s41598-017-07826-0
7. E. I. Cedillo-González, R. Riccò, M. Montorsi, M. Montorsi, P. Falcaro, and C. Siligardi, Build. Environ. **71**, 7–14 (2014). https://doi.org/10.1016/j.buildenv.2013.09.007
8. G. Lofrano, G. Libralato, A. Casaburi, A. Siciliano, P. Iannece, M. Guida, L. Pucci, E. F. Dentice, and M. Carotenuto, Sci. Total Environ. **624**, 461–469 (2018). https://doi.org/10.1016/j.scitotenv.2017.12.145
9. J. Carbajo, A. Bahamonde, and M. Faraldos, Mol. Catal. **434**, 167–174 (2017). https://doi.org/10.1016/j.mcat.2017.03.018
10. A. Pérez-Larios, A. Hernández-Gordillo, G. Morales-Mendoza, L. Lartundo-Rojas, Á. Mantilla, and R. Gómez, Catal. Today. **266**, 9–16 (2016). https://doi.org/10.1016/j.cattod.2015.12.029
11. R. Singh and S. Dutta, Fuel. **220**, 607–620 (2018). https://doi.org/10.1016/j.fuel.2018.02.068
12. J. J. Velázquez, R. Fernández-González, L. Díaz, E. Pulido Melián, V. D. Rodríguez, and P. Núñez, Alloys Compd. **721**, 405–410 (2017). https://doi.org/10.1016/j.jallcom.2017.05.314
13. M. Epifani, E. Comini, R. Diaz, J. Arbiol, et al., "Oxide nanopowders from the low-temperature processing of metal oxide sols and their application as gas-sensing materials," Sens. Actuat. B **118**, 105–109 (2006).
14. R. F. de Farias, U. Arnold, L. Martinez, et al., "Synthesis, characterization and catalytic properties of sol-gel derived mixed oxides," Phys. Chem. Solids. **64** 2385–2389 (2003).

15. D.-S. Lee and T.-K. Liu, "Preparation of $TiO_2$ sol using $TiCl_4$ as a precursor," J. Sol-Gel Sci. Technol. **25** (2), 121–136 (2002).

16. S. Velázquez-Martínez, S. Silva-Martínez, C. A. Pineda-Arellano, A. Jiménez-González, I. Salgado-Tránsito, A. A. Morales-Pérez, and M. I. Peña-Cruz, "Modified sol-gel/hydrothermal method for the synthesis of microsized $TiO_2$ and iron-doped $TiO_2$, its characterization and solar photocatalytic activity for an azo dye degradation," J. Photochem. Photobiol., A **359**, 93–101 (2018).

17. P. Dong, X. Cheng, Zh. Huang, Y. Chen, Y. Zhang, X. Nie, and X. Zhang, "In-situ and phase controllable synthesis of nanocrystalline $TiO_2$ on flexible cellulose fabrics via a simple hydrothermal method," Mater. Res. Bull. **97**, 89–95 (2018).

18. K. Santhi, M. Navaneethan, S. Harish, S. Ponnusamy, and C. Muthamizhchelvan, Applied Surface Science. **500**, 144058 (2020). https://doi.org/10.1016/j.apsusc.2019.144058

19. Y.-Zh. Zheng and M.-L. Zhang, "Preparation and electrochemical properties of nickel oxide by molten salt synthesis," Mater. Lett. **61**. 3967–3968 (2007).

20. Z. Li, Sh. Zhang, and W. E. Lee, "Molten salt synthesis of $LaAlO_3$ powder at low temperatures," J. Eur. Ceram. Soc. **27**, 3201–3205 (2007).

21. Z. Li-hui and H. Qing-wei, "Morphology control of a $\alpha$-$Al_2O_3$ platelets by molten salt synthesis," Ceram. Int. **37**, 249–255 (2011).

22. L. A. Yolshina, "Mechanism of formation of oxide nanopowders by anodic oxidation of metals in molten salts," in *Nanomaterials: Properties, Preparation and Processes* (NOVA, New York, 2011), pp. 255–293.

23. L. A. Elshina, V. Ya. Kudyakov, V. B. Malkov, and N. G. Molchanova, "Creation of thin oxide films and oxide nanopowders by anodic oxidation of metals in molten salts," Russ. J. Inorg. Chem. **53**, 539–544 (2008).

24. L. A. Yolshina, V. B. Malkov, and A. N. Yolshin, "The influence of formation conditions on the electrochemical behavior of lead oxide in sulfuric acid solutions," J. Power Sources **191**, 36–41 (2009).

25. L. A. Yolshina, V. Ya. Kudyakov, V. B. Malkov, and N. G. Molchanova, "Corrosion and electrochemical behavior of aluminum treated with high-temperature pulsed plasma in $CsCl–NaCl–NaNO_3$ melt," Corros. Sci. **53** 2015–2026 (2011).

26. L. A. Elshina and V. A. Elshina, Russ. Metall. No. 2, 138–141 (2020). https://doi.org/10.1134/S0036029520020044

27. L. A. Elshina, V. Ya. Kudyakov, V. B. Malkov, and A. N. Elshin, Glass Phys. Chem. **34** (5) 617–622 (2008). https://doi.org/10.1134/S1087659608050131

28. L. A. Elshina, V. Ya. Kudyakov, V. B. Malkov, and S. V. Plaksin, Prot. Met. Phys. Chem. Surf. **46** (5) 587–592 (2010). https://doi.org/10.1134/S2070205110050151

29. J. Akimoto and H. Takei, "Synthesis and crystal structure of $NaTi_8O_{13}$," J. Solid State Chem. **90** (1), 147–154 (1991).

30. L. A. Yolshina and A. G. Kvashnichev, "Chemical interaction of liquid aluminum with metal oxides in molten salts," Mater. Des. **105**, 124–132 (2016).

*Translated by T. Gapontseva*